Dear Reviewer:

We sincerely thank the reviewer for the valuable and constructive comments on our manuscript “An autonomous cloud detection algorithm using single ground-based infrared radiometer for the Tibetan Plateau” (ID: EGUSPHERE-2025-2876). We have carefully revised the manuscript accordingly. Below, we provide point-by-point responses (reviewer’s comments in italic, our responses in normal font).

Q1. *Recent advancements of cloud detection in the Tibetan Plateau regions can be considered in the Introduction.*

Response: Thank you for your suggestion. The recent advancements in cloud detection have been added to the introduction. “Since the 1980s, meteorological satellites such as CloudSat, CALIPSO, Himawari-8, and FengYun-4A have been used to reveal cloud characteristics over the Tibetan Plateau (Yan et al., 2019; Yi, 2019; Wang et al., 2020; Liu et al.,2021). In contrast to these top-down observations, ground-based instruments—including cloud radars, lidars, and all-sky imagers—provide essential bottom-up data for validating satellite products and investigating local cloud properties in greater detail (Song et al., 2017; Huo et al., 2021; Luo et al., 2024; Zhao et al., 2024).” **(**Line 44-50, Section 1, Page 3)

Q2. *To enhance clarity, authors may consider presenting a comprehensive flowchart that displays the primary algorithm's logic and main steps. While Figure 7 illustrates the algorithm flow, it would be beneficial to include additional details described in the text, such as the steps of normalization and the calculation of the clear-sky IRBT diurnal cycle. This comprehensive visualization would assist readers in understanding the entire algorithm. In addition, Figure 7 can be repositioned to appear earlier in the methodology section.*

Response: According to your suggestion, we revised the flow chart, which involves more details in normalization, calculation and threshold used (Fig. R1). (Page 16)

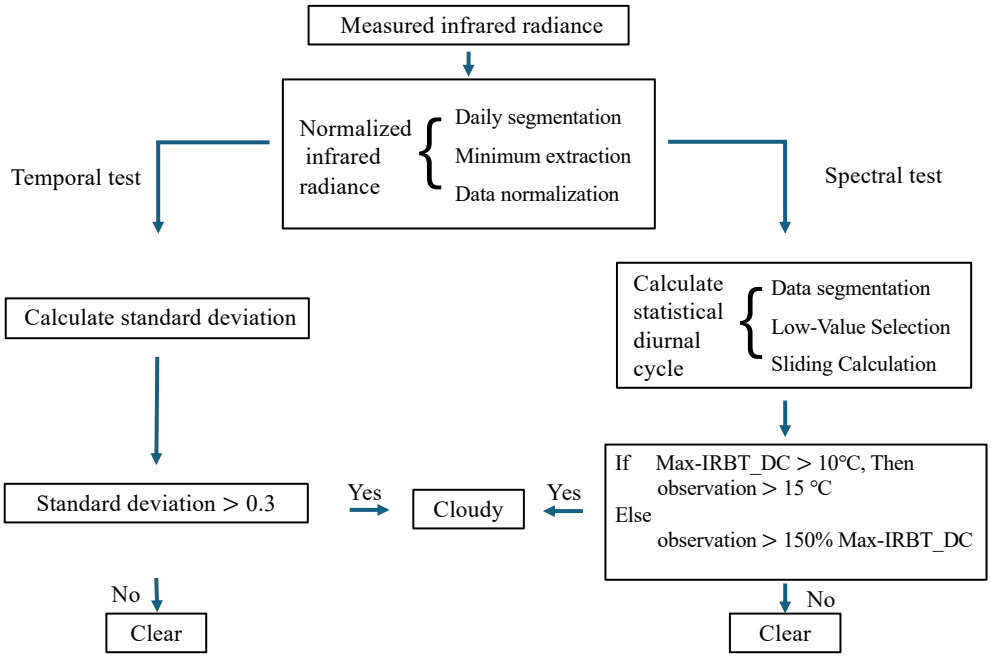

Fig. R1 Flow chart of the cloud detection algorithm.

The flow chart serves as a summary of the previously described algorithmic process. Figures 8 and 9 then present the corresponding step-by-step results and final determination for a specific case, which directly support the flow chart. Therefore, we believe its current placement is more appropriate.

Q3. *In Section 2.1, it is recommended that authors present a figure or table summarizing the instrument information, its surrounding environment (e.g., location, elevation), and typical sky conditions.*

Response: According to your suggestions, we added a table to Section 2.

Measurement specifications	
Temperature range:	-50~400 ℃
Spectral range:	9.6~11.5 μm
Measurement uncertainty:	±0.5 ℃ plus 0.7 % of the temperature difference between measured target and instrument
Long-term stability:	Better than 0.01 % of the absolute measured temperature per month
Deployment environment	
Location:	A rooftop platform at Tibet University's Najin campus
Elevation:	3650 meters

Table R1: The measurement parameters and deployment environment of the infrared radiometer.

Q4. *Thresholds used in the section 3.2 and section 3.4 need to be clarified, such as 150% of the maximum and the lowest 5% of IRBT values. Authors may provide a brief discussion on how these thresholds were determined.*

Response: Thank you for your comment. In the extraction of the clear-sky IRBT diurnal cycle, the wet season window is doubled to capture more clear-sky data due to prolonged cloud cover. The temporal resolution of the clear-sky IRBT diurnal cycle is 20 minutes during the wet season and 10 minutes otherwise, compared to the 2-second observed IRBT resolution. Each window thus contains 600 (wet season) or 300 (other seasons) data points, ensuring statistical confidence. To mitigate cloud contamination, the lowest 5% of IRBT values are averaged as the diurnal cycle value for the target time—using 30 values in the wet season and 15 otherwise. Here the 5% setting is an empirical value, which cannot be justified under the current conditions without other supplementary observations, but works well in practice. Corresponding discussion has been added in the paper. **(**Line 188-191, Section 3.2, Page 11)

Following your suggestion, we reassessed the sensitivity of the results to the choice of thresholds. For the spectral test, we adjusted the threshold settings to account for seasonal variations. Due to diurnal temperature variations in different season, the clear-sky IRBT diurnal cycle exhibits seasonal differences. For example, the average maximum IRBT of the clear-sky diurnal cycle (Max-IRBT_DC) in June and November 2021 was 5.86 and 10.6 ℃, respectively. Using a uniform 150% increase would result in a high threshold in winter, potentially leading to misjudgments of thin high clouds. Therefore, in the algorithm, when the Max-IRBT_DC exceeds 10℃, the threshold is automatically set to 15℃; otherwise, the threshold is set to 150% of Max-IRBT_DC.

The corresponding revisions have been incorporated into the manuscript. **(**Line 210-213 Section 3.2, Page 12) **(**Line 277-279, Section 3.4, Page 17)

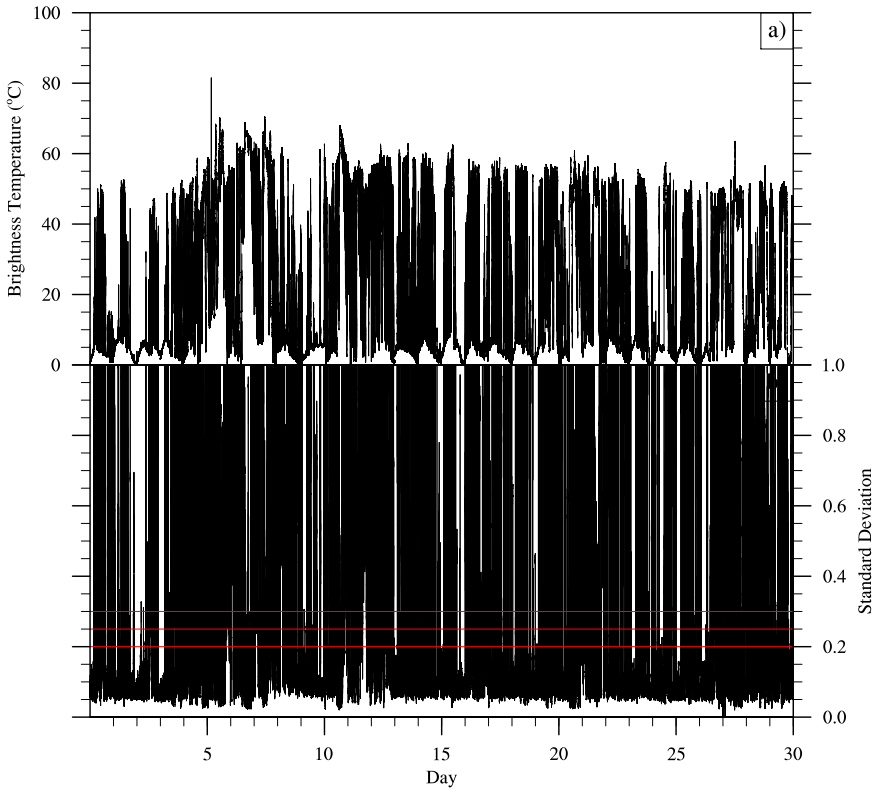

Fig. R2 The normalized infrared brightness temperatures (top) and the corresponding calculated standard deviations (bottom) in June 2021. Red reference lines represent the three thresholds - 0.2, 0.25 and 0.3.

For the temporal test, we performed a sensitivity analysis with thresholds of 0.2, 0.25, and 0.3. The results show that during the wet season, the choice of these thresholds has little effect on detection outcomes, as clouds typically exhibit much larger standard deviations (Figs. R2–R3). In winter, the threshold setting may affect the classification in a small fraction of cases (Fig. R4). We further analyzed specific cases, such as November 3, 2021, shown in Fig. R5. Although the IRBT indicates clear skies (top figure), the standard deviation increased to between 0.2 and 0.3 from 4 to 8 UTC (bottom figure). However, without complementary cloud observations, we cannot determine with certainty whether the small fluctuations in standard deviation around 0.2–0.3 were due to clouds or other factors. Based on this sensitivity analysis, we adopt a threshold of 0.3 for cloud detection.

The result of sensitivity analysis has been added in the manuscript. **(**Line 245-253, Section 3.3, Page 15)

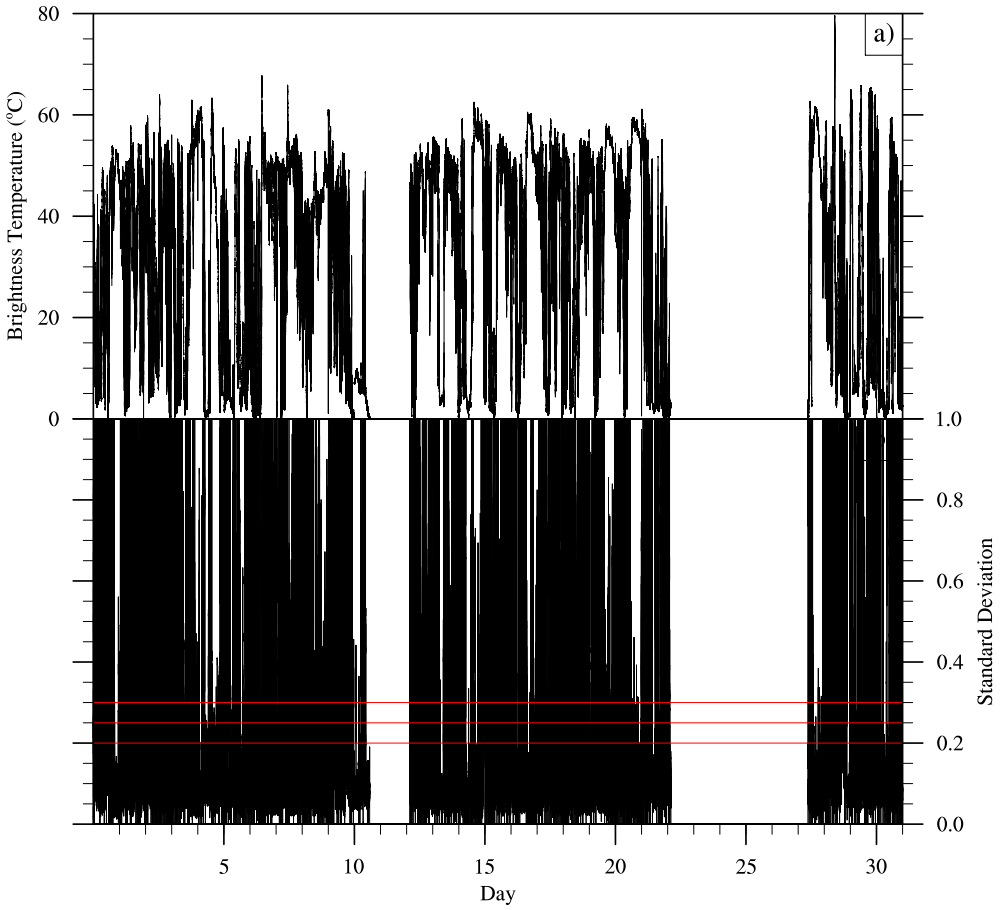

Fig. R3 The normalized infrared brightness temperatures (top) and the corresponding calculated standard deviations (bottom) in July 2021. Red reference lines represent the three thresholds - 0.2, 0.25 and 0.3.

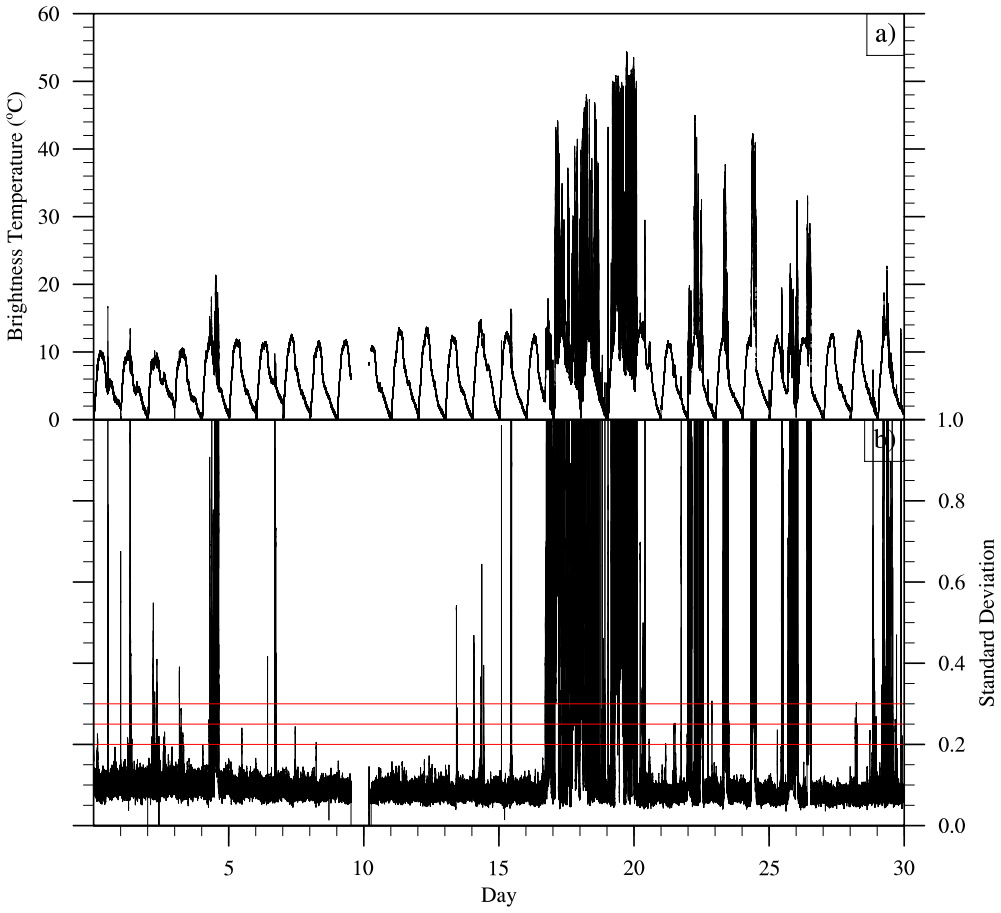

Fig. R4 The normalized infrared brightness temperatures (top) and the corresponding calculated standard deviations (bottom) in November 2021. Red reference lines represent the three thresholds - 0.2, 0.25 and 0.3.

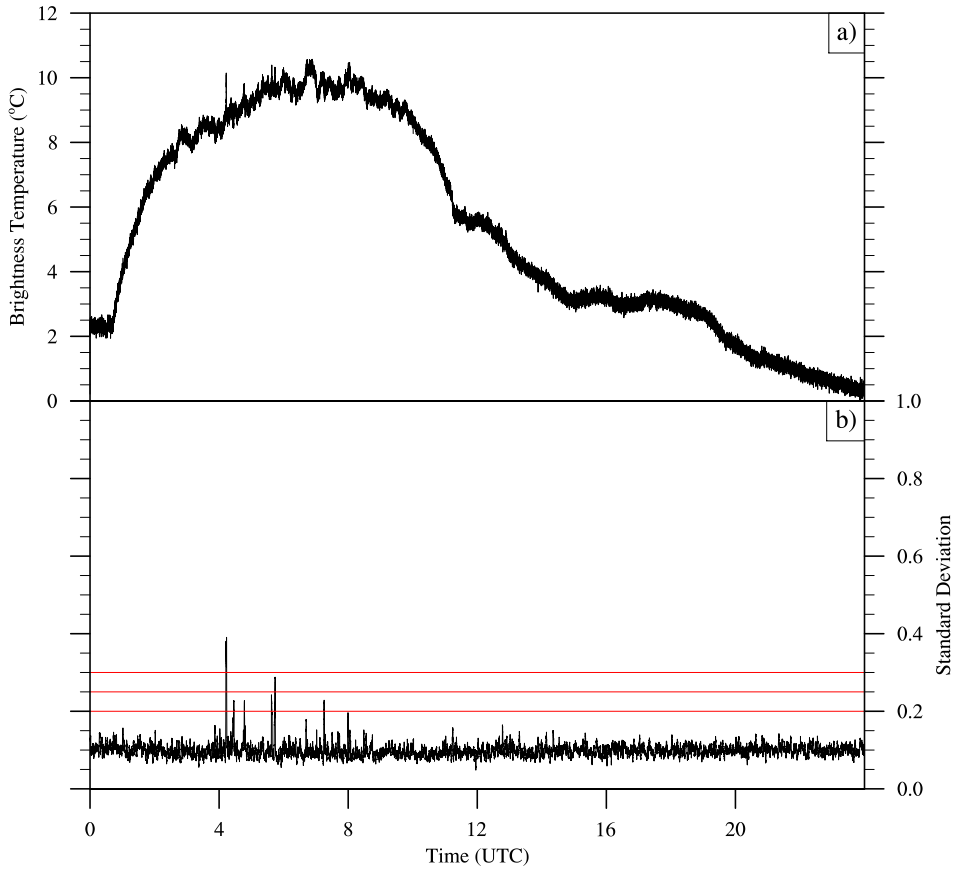

Fig. R5 The normalized infrared brightness temperatures (top) and the corresponding calculated standard deviations (bottom) on November 03, 2021. Red reference lines represent the three thresholds - 0.2, 0.25 and 0.3.

Q5. *Some errors should be corrected:*

Line 58: ‘ too weak to reliably distinguish’-> ‘too weak to be reliably distinguished’

Line 62: ‘that combines’-> ‘that combined’

Line 248: ‘and are shown’-> ’are shown‘

Response: Thank you for your reminding. The above grammatical errors have been corrected.

References

Huo, J., Bi, Y. H., Liu, B., Han, C. Z., and Duan, M. Z.: A dual-frequency cloud radar for observations of precipitation and cloud in Tibet: Description and preliminary measurements, Remote Sensing, 13, 4685, https://doi.org/10.3390/rs13224685, 2021.

Luo, J., Pan, Y., Su, D., Zhong, J., Wu, L., Zhao, W., Hu, X., Qi, Z., Lu, D., and Wang, Y.: Innovative cloud quantification: deep learning classification and finite-sector clustering for ground-based all-sky imaging, Atmos. Meas. Tech., 17, 3765–3781, https://doi.org/10.5194/amt-17-3765-2024, 2024.

Liu, B., Huo, J., Lyu, D., and Wang, X.: Assessment of FY-4A and Himawari-8 cloud top height retrieval through comparison with ground-based millimeter radar at sites in Tibet and Beijing, Adv. Atmos. Sci., 38, 1334−1350, Song, X. Q., Zhai, X. C., Liu, L. P., and Wu, S. H.: Lidar and ceilometer observations and comparisons of atmospheric cloud structure at Nagqu of Tibetan Plateau in 2014 Summer, Atmosphere, 8, 9, https://doi.org/10.3390/atmos8010009, 2017.

Song, X. Q., Zhai, X. C., Liu, L. P., and Wu, S. H.: Lidar and ceilometer observations and comparisons of atmospheric cloud structure at Nagqu of Tibetan Plateau in 2014 Summer, Atmosphere, 8, 9, https://doi.org/10.3390/atmos8010009, 2017.

Yan, Y. F., and Liu,Y. M.: Vertical structures of convective and stratiform clouds in boreal summer over the Tibetan Plateau and its neighboring regions, Adv. Atmos. Sci., 36,1089−1102, https://doi.org/10.1007/s00376-019-8229-4, 2019.

Yi, M. J.: Differences in cloud vertical structures between the Tibetan Platea and Eastern China Plains during rainy season as measured by CloudSat/CALIPSO, Advances in Meteorology, 6292930, https://doi.org/10.1155/2019/6292930,2019.

Wang, Y. J., Zeng, X. B., Xu, X. D., Welty, J., Lenschow, D. H., Zhou, M. Y., and Zhao, Y.: Why are there more summer afternoon low clouds over the Tibetan Plateau compared to eastern China? Geophys. Res. Lett., 47, e2020GL089665, https://doi.org/10.1029/2020gl089665, 2020.

Zhao, W., Wang, Y., Bi, Y., Wu, X., Tian, Y., 2, Wu, L., Luo, J., Hu, X., Qi, Z., Li, J., Pan, Y., and Lyu, D.: Unveiling cloud vertical structures over the interior Tibetan Plateau through anomaly detection in synergetic lidar and radar observations, Adv. Atmos. Sci., 41(12), 2381−2398, https://doi.org/10.1007/s00376-024-3221-z, 2024.